Calculation of Various Diffuser Flows with Inlet Swirl and Inlet Distortion Effects

C. Hah*
General Electric Company, Schenectady, New York

A method of predicting the properties of various turbulent flows in planar, conical, and annular diffusers with inlet swirl and inlet distortion effects has been developed and appraised. The numerical scheme is based on the fully conservative control volume representation of governing conservation equations. The method is capable of carrying out the calculation when the flowfield contains stalled or recirculation flow regions. Three different discretization schemes are compared to analyze the numerical diffusion. An algebraic Reynolds stress model is used to represent the large streamline curvature. The appraisal is achieved by comparing predicted results with various experimental data. The results show that the numerical scheme with the utilized turbulence closure model predicts various diffuser flows with the effects of inlet swirl and inlet distortion within measurement accuracy and is able to provide various guiding information for many engineering applications.

Nomenclature

C_{prs} = diffuser performance coefficient based on area averaged pressure, Eq. (17)
C_{pw} = diffuser performance coefficient based on wall static pressures, Eq. (16)
$C_s, C_{\phi 1}, C_\mu, C_{\epsilon 2}, \delta_k, \delta_\epsilon, \gamma$ = constants in turbulence closure models
g_{ij}, g^{ij} = metric tensor
k = turbulence kinetic energy
P = $-\overline{u_i u_j} U^i_{,j}$
p = static pressure
S = production in the energy dissipation equation
U, V, W = axial, radial, and circumferential mean velocities
u, v, w = axial, radial, and circumferential fluctuating velocities components, Eq. (2)
U^i, u^i = contravariant mean and fluctuating velocity
τ_w = wall shear stress
Γ = diffusion coefficient, Eq. (10)
δ_{ij} = Kronecker delta
ν = kinematic viscosity
ρ = density

Subscripts

1 = diffuser inlet value
2 = diffuser exit value
c = diffuser centerline value
f = value at the node next to solid wall

Superscripts

$\bar{(\ )}$ = average value
$(\ )'$ = fluctuating quantity

I. Introduction

DIFFUSERS are widely used for converting kinetic energy to pressure, and a reliable prediction method of diffuser flows with practical shape and flow conditions will lead to the design of the fluid machine with improved efficiency.

The literature contains many experimental studies of diffuser performance. Kline et al.,[1] Sovran and Klomp,[2] and Bradley and Cockrell[3] investigated diffuser flows with relatively small total diverging angles (4-12 deg). For uniform inlet flows, the effect of geometry on the performance of various diffusers is fairly well established and reliable prediction methods have been developed, e.g., Ghose and Kline[4] and Bardina et al.[5]

It has been well known that certain types of inlet distortion increase diffuser pressure recovery coefficients. The swirling inlet velocity component in the diffuser is often observed in flow downstream of the gas turbine or certain types of combustor chambers. The effect of inlet swirl on conical diffusers was experimentally studied by McDonald et al.[6] and Senoo et al.[7] With the swirling velocity component, the flow is pressed toward the wall by the centrifugal force and the wall boundary layer is less likely to separate even if the divergence angle of diffuser is large, and a high-pressure recovery coefficient is observed. However, excessive amounts of swirl reduces the axial velocity too far near the centerline of the diffuser or induces a reversed flow region, which results in a low-pressure recovery rate.

Moore and Kline,[8] Sajben et al,[9] and Hoffmann[10] altered inlet velocity and turbulence characteristics to improve the overall diffuser efficiency. With the inlet flow control device (passive rod or vortex generator), the high-energy fluid outside the wall boundary layer of the diffuser is mixed with the low-energy fluid inside the boundary layer to delay the separation and to maintain large effective area. The possibility of predicting these flows with the effects of inlet swirl and inlet distortion has not been previously explored in detail and is the subject of the present study.

The present investigation is aimed at developing and testing a numerical method to calculate turbulent flows in various diffusers with the effects of inlet swirl and inlet distortion. It can be applied to flows with and without separation.

In order to obtain useful numerical predictions for the complex turbulent flows, the problem of reducing the numerical diffusion and using proper turbulence closure models should be carefully addressed. Various previous studies[11-13] have shown that the simple central-upwinding hybrid discretization of convection terms leads to significant error in the solution when the flow is skewed relative to the numerical mesh and the cell Pecklet number exceeds two. Also the numerical diffusion obscures physical processes and makes the assessment of the turbulence closure scheme very difficult. Higher order discretization schemes are used and evaluated for the present diffuser flow problems.

It has been well known that the turbulent recirculating flow in various geometries is very strongly affected by the streamline curvature. Various studies have indicated that the numerical solution underpredicts the recirculating zone by up

Presented as Paper 82-1003 at the AIAA/ASME Third Joint Thermophysics, Fluids, Plasma and Heat Transfer Conference, St. Louis, Mo., June 7-11, 1982; submitted June 7, 1982; revision received Nov. 16, 1982.

*Fluid Mechanics Engineer, Fluid Mechanics and Combustion Branch, Mechanical Systems and Technology Laboratory, Corporate Research and Development. Member AIAA.

to 20% when the turbulence model does not account for the curvature effect correctly. Durst and Rastogi[14] and Leschziner and Rodi[15] used curvature modifications in two-equation and algebraic Reynolds stress models. Durst and Rastogi used the Richardson number to represent the curvature effect empirically. The correction is qualitative and probably cannot be used for a wide range of flows. Leschziner and Rodi simplified the Reynolds stress model to include curvature correction in the algebraic Reynolds stress model. However, their derivation of the relationship between stress and strain for curved shear flow is based on rather unrealistic assumptions and the correction is not tensor invariant. Also the calculation of local radius of curvature and streamwise velocity gradient for the estimation of the effective eddy viscosity is very difficult when multicomponents of curvature are involved (such as the diffuser flow with swirl). For the present study, an algebraic Reynolds stress model with tensor-invariant curvature correction is used. The curvature correction can be easily used for highly complex flow with multiple curvature components.

In the next section, the governing equations and the turbulence closure modeling are described. Higher order discretization schemes and solution procedures are discussed in Sec. III. Numerically predicted results are presented and compared with the measurements in Sec. IV. The conclusions drawn from this study are given in the last section.

II. Governing Equations and Turbulence Closure Modeling

The equations governing the flows considered, in generalized tensor form, are as follows

$$U^i_{,i}=0, \qquad u^i_{,i}=0 \tag{1}$$

$$U^j U^i_{,j}+u^j u^i_{,j}=-\frac{g^{ij}}{\rho}\frac{\partial p}{\partial x^j}+\nu g_{jk}U^i_{,jk} \tag{2}$$

where U^i and u^i are the mean and fluctuating contravariant velocity components, respectively. The component equations for a specific coordinate system can be written with the fundamental metric tensor and the Christoffel symbols of the coordinates.

To get closure of the above system of equations, the turbulence stress term $\overline{u^iu^j}$ should be described with proper means. For the present study, the stress terms are evaluated with the following simplified transport equation of the Reynolds stress,

$$0=(1+C_1)\,(-\overline{u_ku^j}U^i_{,k}-\overline{u_ku^i}U^j_{,k})\,(1-\gamma) - \tfrac{2}{3}g^{ij}\epsilon(1-\gamma)-C_{\phi 1}(\epsilon/k)\,(\overline{u^iu^j}-\tfrac{2}{3}g^{ij}k) \tag{3}$$

where $P=-\overline{u_iu_j}U^i_{,j}$ and C_1 is a variable which relates the collective effects of the convection and diffusion terms to the production term. The physical basis of Eq. (3) is explained in Ref. 16. As the convection and the diffusion terms of the Reynolds stress transportation equation are approximated collectively with the variable C_1, the Reynolds stress components can be evaluated when the values of k, ϵ, and $U^i_{,j}$ are given. Therefore, only two additional transport equations for the turbulence kinetic energy and the energy dissipation rates are required for the estimation of Reynolds stresses. With the present model, the collective effect of convection and diffusion (A_{ij}) is related to the transportation of the turbulence kinetic energy ($P-\epsilon$) by

$$A_{ij}=(P_{ij}/P)\,(P-\epsilon) \tag{4}$$

where

$$P_{ij}=-\overline{u_ku^j}U^i_{,k}-\overline{u_ku^i}U^j_{,k}$$

and the variable C_1 can be expressed as

$$C_1=(\epsilon/P)-1 \tag{5}$$

The distribution of k and ϵ, which is required for the solution of Eq. (3) is determined by solving the following transport equations,

$$U^i\frac{\partial k}{\partial x^i}=\frac{\partial}{\partial x^i}\left(\frac{\nu_{\text{eff}}}{\sigma_k}\frac{\partial k}{\partial x^i}\right)+P-\epsilon \tag{6}$$

$$U^i\frac{\partial \epsilon}{\partial x^i}=\frac{\partial}{\partial x^i}\left(\frac{\nu_{\text{eff}}}{\sigma_\epsilon}\frac{\partial \epsilon}{\partial x^i}\right)+S-C_{\epsilon 2}\frac{\epsilon^2}{k} \tag{7}$$

where $\nu_{\text{eff}}=C_\mu k^2/\epsilon$, $k=\frac{1}{2}g_{ij}\overline{u^iu^j}$ and S is the source term of the energy dissipation equation. The following form of S has been widely used to balance the equation after the similarity with the turbulence energy equation,

$$S=C_{\epsilon 1}(\epsilon/k)P \tag{8}$$

Many numerical studies have shown that the set of Eqs. (6-8) does not describe the curved turbulent flow adequately. The effect of the streamline curvature is to decrease the turbulent transportation when the angular momentum increases with the radius of the streamline curvature and vice versa for the opposite case. For the curved flow, the production of the turbulence kinetic energy [the term P in Eq. (6)] is increased or decreased due to the extra strain rate, depending on the stabilizing or destabilizing effect of the curvature. Therefore, the effect of the streamline curvature is properly represented in the turbulence energy equation. The transport equation of the energy dissipation rate is based on rather unproven assumptions and the use of the production of the turbulence kinetic energy as the primary source term results in poor prediction for the curved flow. The characteristic turbulence length scale is proportional to k^2/ϵ and this length scale does not change with the streamline curvature when Eq. (8) is used as a source in the energy dissipation equation.

To represent the curvature effect properly, the anisotropy in Reynolds stress is used as the source term,

$$S=C_S\frac{\epsilon^2}{k^3}\,(\overline{u^iu^j}-\tfrac{2}{3}k\delta_{ij})\,(\overline{u^ju^i}-\tfrac{2}{3}k\delta_{ji}) \tag{9}$$

As the above expression does not include a mean strain rate, the energy dissipation rate is not directly affected by the extra strain rate and the change of the length scale due to the streamline curvature is properly represented. Various constants in the transport equations of the turbulence quantities are $C_\mu=0.09$, $C_{\phi 1}=1.5$, $C_S=1.8$, $C_{\epsilon 2}=1.44$, $\delta_k=1.0$, $\delta_\epsilon=1.22$, and $\gamma=0.6$. The above turbulence closure model has been successfully applied to predict a highly curved free shear layer.[17]

III. Higher Order Discretization Scheme and Solution Procedure

The governing momentum conservation equations and the transport equations for the turbulence quantities can be expressed in the following form for the convenience of the formulation

$$(\rho U_i\phi)_{,i}=(\Gamma\phi_{,i})_{,i}+S_\phi \tag{10}$$

where ϕ is any of the dependent variables (U, V, W, k, or ϵ) and Γ the diffusion coefficient, and S_ϕ encompasses all remaining terms. The finite-difference equations are formulated by integrating the above differential equations over the control volume. The mean velocity field and turbulence quantities are solved simultaneously with the assumed pressure field and adjustments are made to the pressure field to insure mass conservation. The overall procedure is an iterative and line-by-line procedure. Since the procedure has been described in various references (e.g., Patankar,[18] Gosman and Pun[19]), attention is focused here on the discretization of the convection term and numerical diffusion.

As is well known, the central differencing of the convection term gives a second-order truncation error, but the scheme is unstable when the cell Peclet number exceeds two. Consequently, unrealistically refined grids are required for a stable solution. Upwind or hybrid discretizations for convection terms have been widely used as an alternative. Although the upwind differencing gives a stable solution regardless of the cell Peclet number, excessive numerical diffusion is generated during the solution procedure. The numerical diffusion is the function of the grid size and the skewness between the grid line and the velocity vector. To reduce the numerical diffusion and obtain an accurate solution with the upwind discretization, the number of grid points increases to too large a number to accommodate for any practical calculation. Several alternate discretization schemes have been proposed to obtain acceptable solutions with a practically sized computation grid. The quadratic upstream interpolation scheme by Leonard[20] and the skew-upwinding scheme by Raithby[21] have been properly modified for the present solution procedure. Figure 1 shows how to estimate the values of the dependent variable at the surface of the control volume. With the quadratic upstream interpolation scheme, the value of ϕ_e at the surface e is given as follows,

$$\text{if } U_e \geq 0,\ \phi_e = \tfrac{1}{2}(\phi_i + \phi_{i+1}) - \tfrac{1}{8}(\phi_{i-1} + \phi_{i+1} - 2\phi_i) \quad (11a)$$

$$\text{if } U_e < 0,\ \phi_e = \tfrac{1}{2}(\phi_i + \phi_{i+1}) - \tfrac{1}{8}(\phi_i + \phi_{i+2} - 2\phi_{i+1}) \quad (11b)$$

The second terms on the right-hand sides of Eqs. (11a) and (11b) can be interpreted as a correction due to the respective upstream weighted curvatures. If these terms are omitted, the central difference form is recovered. Although this scheme is claimed to possess higher accuracy and more stable convective sensitivity, the scheme is not unconditionally stable, especially when turbulent flows with high Reynolds numbers are computed with relaxation-type algorithms. To insure convergence with the present solution procedure, the following decompositions of the difference formula were used in which the last two quantities are handled as extra source terms and evaluated with the values of the previous iteration,

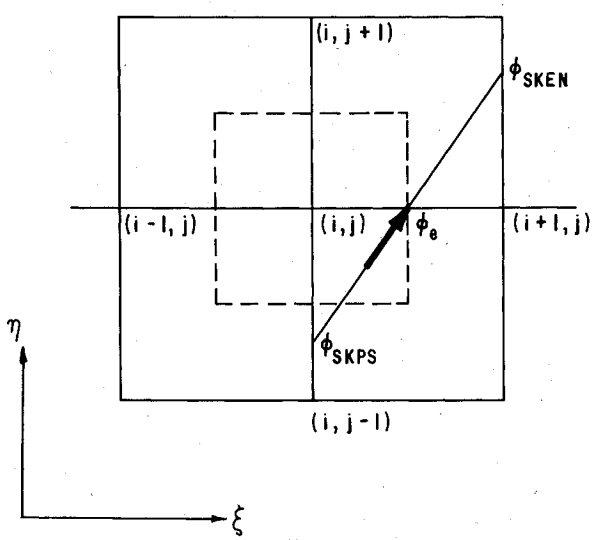

Fig. 1 Grid notation for higher order scheme.

$$\text{if } U_e \geq 0,\ \phi_e = \frac{6}{8}\phi_i + \frac{2}{8}\phi_{i+1} + \frac{1}{8}(\phi_{i+1} - \phi_{i-1}) \quad (11c)$$

$$\text{if } U_e < 0,\ \phi_e = \frac{6}{8}\phi_{i+1} + \frac{2}{8}\phi_i + \frac{1}{8}(\phi_i - \phi_{i+2}) \quad (11d)$$

With Eqs. (11c) and (11d), the solution converges when the cell Peclet number is less than four without any possible wiggles in the solution.

The skew-upwinding scheme by Raithby[21] is aimed primarily at reducing the error due to the streamline-to-grid skewness. The value of dependent variables at the control volume surface is assessed by performing upwind differencing on the true streamline. The value of ϕ_e is determined as

$$\phi_e = \phi_{SKPS} \text{ if } U_e \geq 0$$

$$\phi_{SKEN} \text{ if } U_e < 0 \quad (12)$$

for the streamline shown in Fig. 1 and unknown values at nine nodal points are interpolated for the formulation.

The inlet boundary conditions were taken from the measurement where possible. The distribution of the turbulence kinetic energy at the inlet was estimated using the equilibrium theory when experimental values were not available. The rate of energy dissipation at the inlet section was not available for all cases and the value was estimated using a fixed length scale at the inlet with the expression,

$$\epsilon = C_\mu k^{(3/2)}/L \quad (13)$$

where L is the characteristic length scale and $L = 0.01L_1$ (L_1 is the inlet pipe radius or inlet channel height). At the exit plane, all of the streamwise gradients of unknown variables were presumed to be constant and overall mass conservation through each cross section was imposed. The wall function was used to reduce the number of grid points near the wall. At nodes nearest to the solid walls, the velocity vector is assumed to be on the plane parallel to the solid walls and local equilibrium is assumed for the turbulence quantities. The node next to the diffuser wall is located $0.001L_1$ away from the wall and well inside the inertial sublayer ($30 < y_f\sqrt{\tau_w/\rho}/\nu < 400$). The value of the turbulence kinetic energy at this node (k_f) is estimated from the transport equation of the turbulence kinetic energy with the convective and diffusive effects through the wall neglected. The rate of energy dissipation at this node is obtained from the expression,

$$\epsilon_f = A(C_\mu^{3/4} k_f^{3/2})/y_f \quad (14)$$

where y_f is the distance from the wall and $A = 2.4$.

The fluctuations of the total mass flow rate at each axial plane are monitored during iteration and when the total mass flow residual divided by the inlet mass flow rate is less than 10^{-4}, the solution is assumed to be converged. About 4. 6 s is required per iteration on a VAX 11/780 with 50×40 nodes and the solution coverges with less than 650 iterations.

IV. Comparison between the Numerical Predictions and the Measurements

In this section, selected numerical predictions are presented and compared with the measurements for three sets of experimental data on the diffuser flow with the effects of the inlet swirl and the inlet distortion.

Comparison of the Effects of the Rankine-Vortex Type of Swirl

The experimental data on the effect of the swirl by Senoo, Kawaguchi, and Nagata[7] are used for comparison purposes. The measurements were done with five different conical diffusers (total divergence angles of 8, 12, 16, 20, and 30 deg) to clarify the influence of swirl on the pressure recovery coefficient. The Reynolds number at the diffuser inlet was up to 4.5×10^5. The following dimensionless parameter was used to express the intensity of the swirl,

$$m=\int_0^R UWr^2\mathrm{d}r\Big/R\int_0^R U^2r\mathrm{d}r \tag{15}$$

where U and W are the axial and the circumferential velocity components and r is the radial position. Four different swirl intensities ($m=0.0$, 0.07, 0.12, and 0.18) were tested for each diffuser configuration. The detailed velocity measurements were reported at the inlet of the diffuser and at the sections where the area ratio is 4.0 in addition to pressure recovery coefficients. The distribution of the circumferential velocity component at the inlet section is very similar to that of the Rankine vortices. The outer part of the circumferential velocity profile is a free vortex pattern with the smaller inner part of a solid vortex pattern.

The computation was performed with 50×40 nodes and the employed grid is shown in Fig. 2. Simple exponential stretching is employed on each axial grid line. The grids were clustered both near the diffuser wall and near the diffuser centerline for a better description of the wall boundary layer and the stagnation bubble near the centerline. The predicted developments of the axial velocity profile with and without inlet swirl for the total divergence angle of 16 deg are given in Fig. 3. The development of the circumferential velocity profile is shown in Fig. 4. The predicted axial velocity profiles indicate that there exists a small flow separation near the diffuser wall at the diffuser exit which the measurement does not show clearly. The velocity profile was measured with a five-hole probe which cannot detect the thin stalled flow region accurately, and the disagreement between the measurement and the prediction can be safely regarded to be in the range of measurement error. As shown in Fig. 3, the numerical prediction indicates that there exists a stalled flow region near the centerline of the diffuser when inlet swirl intensity is high. With the strong swirl, a large solid vortex core is developed at the center and a low-pressure region is created near the centerline. When the difference between the wall static pressure and the centerline static pressure becomes greater than the dynamic pressure of the axial flow, a stagnation or backflow region is formed at the centerline. Harvey[22] and So[23] also observed experimentally the reversed flow region near the centerline when the flow has a strong swirl.

Figure 5 shows the comparison for the pressure recovery coefficients which is defined as

$$C_{pw}=(p_{S2}-p_{SI})/p_{DI} \tag{16}$$

where p_{SI} is the wall pressure at the inlet section, p_{S2} the wall pressure at the exit section, and p_{DI} the dynamic pressure of the mean axial velocity at the inlet section.

To evaluate the effects of the numerical diffusion and the streamline curvature effects, the flow was also computed with the different discretization schemes and the standard k-ϵ turbulence closure model. The predicted results with different discretization schemes and the turbulence closure models are also compared in Fig. 5. With the 50×40 node, the quadratic upstream interpolation scheme and the skew-upwinding scheme gave very similar results but only the results with the skew-upwinding scheme are presented.

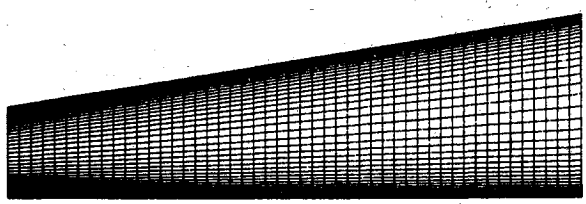

Fig. 2 Computational grid.

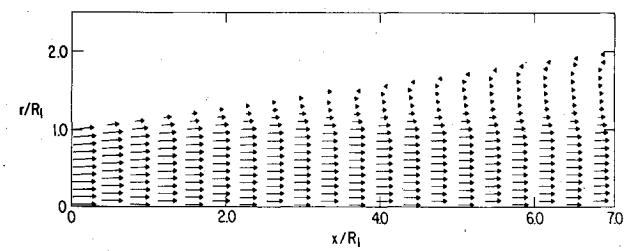

Fig. 3a Development of axial velocity profile with no swirl.

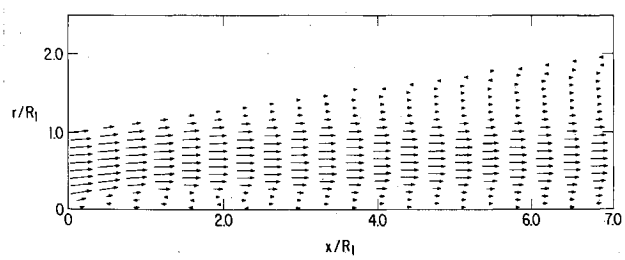

Fig. 3b Development of axial velocity profile with swirl ($m_I=0.18$).

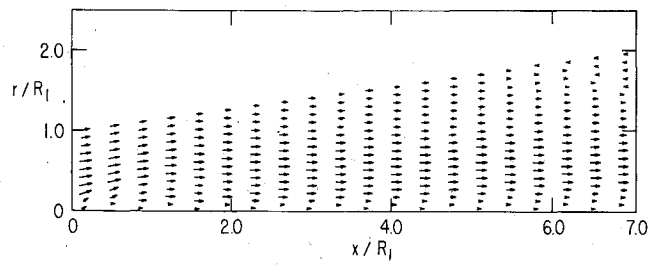

Fig. 4 Development of circumferential velocity profile with swirl.

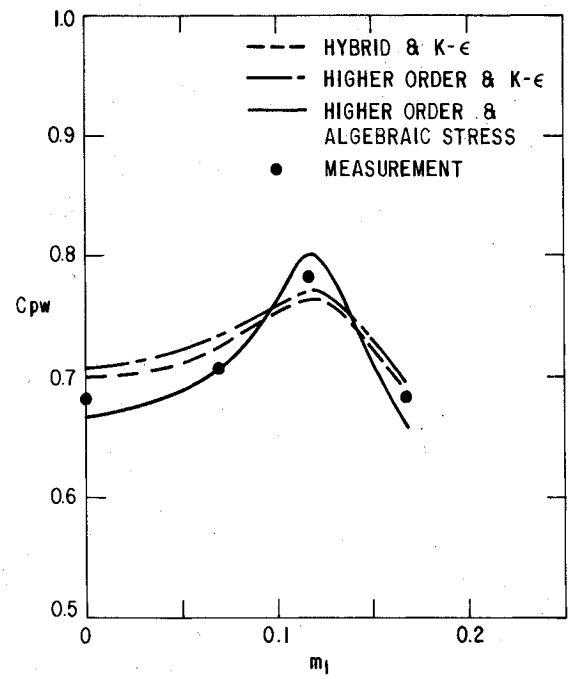

Fig. 5 Comparison for the pressure recovery coefficient.

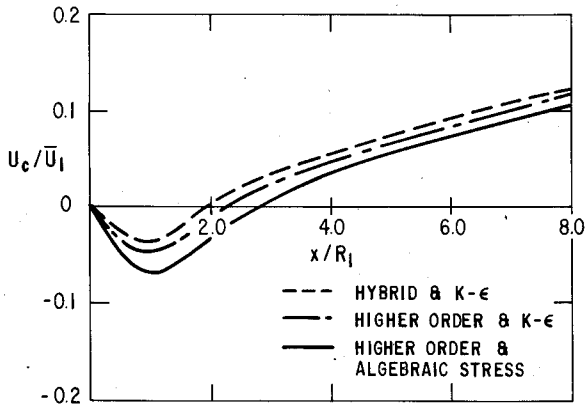

Fig. 6 Comparison for the diffuser centerline velocity.

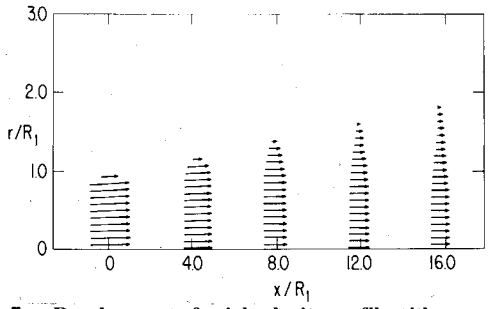

Fig. 7a Development of axial velocity profile with no swirl.

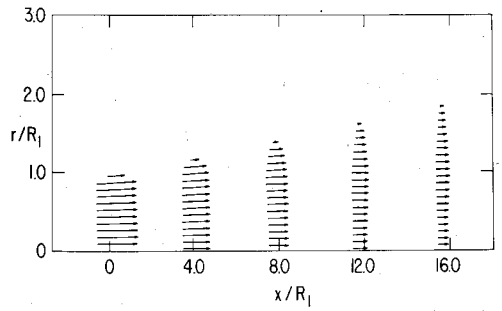

Fig. 7b Development of axial velocity profile with swirl (maximum swirl angle, 22 deg).

As shown in Fig. 5, there exists an optimum amount of swirl for the pressure recovery coefficient. With the swirling velocity component, the flow inside the diffuser is pressed toward the wall and the boundary-layer development and the flow separation along the diffuser wall is suppressed. However, the strong swirl also creates a very low-velocity or reversed velocity region near the centerline and the effective area for pressure rise is decreased. All these effects are very well predicted when the higher order discretization scheme and the algebraic Reynolds stress model are used. The comparison of the results by the hybrid scheme and the higher order discretization schemes indicates that the calculation with the hybrid scheme predicts lower pressure recovery compared to that with a higher order scheme. With the hybrid scheme, the additional numerical diffusion tends to increase the boundary-layer thickness and the lower pressure recovery is obtained. For the present flow, the angular momentum decreases along the radius of curvature near the wall and the effect of the streamline curvature is to enhance the turbulent mixing near the wall. Therefore, lower pressure recovery is obtained due to the streamline curvature.

When a reversed flow region is created near the centerline, the angular momentum increases along the radius of curvature and the turbulent transportation is decreased due to the effect of the streamline curvature. The size of the recirculating zone is underestimated substantially when the hybrid scheme

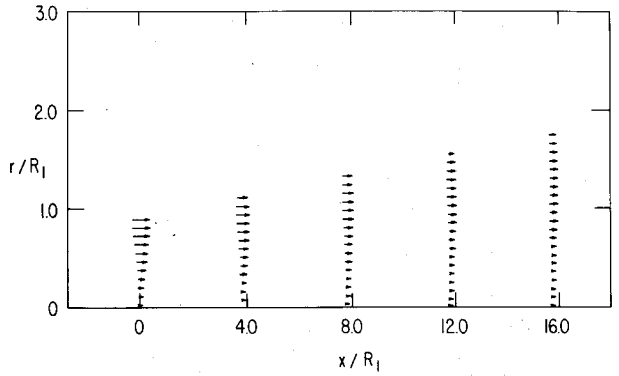

Fig. 8 Development of circumferential velocity profile with swirl (maximum swirl angle, 22 deg).

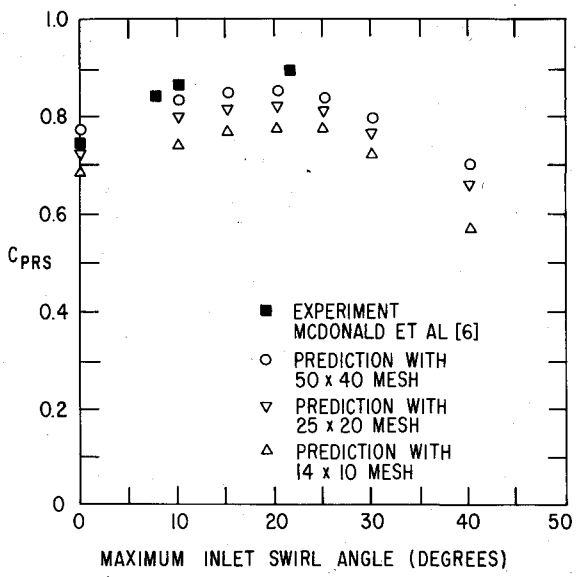

Fig. 9 Comparison for the pressure recovery coefficient.

with the standard k-ϵ equations are used for the prediction. The curvature-corrected algebraic Reynolds stress model predicts all of these curvature effects correctly and the predictions agree with the experimental data. The diffuser centerline velocity distributions for the strong swirl are compared in Fig. 6.

The hybrid scheme underestimates the bubble size by almost 30% and the higher order scheme with the standard k-ϵ turbulence model underpredicts the bubble size by about 15%. for the present flow, the effect of the streamline curvature is to promote the turbulent mixing near the wall. When the hybrid scheme with the standard k-ϵ model is used, the numerical diffusion enhances the development of the wall boundary layer and the predicted pressure recovery coefficients look more like the measurements than the results of the higher order scheme with the standard k-ϵ mode. This is due to an excessive amount of numerical diffusion and not due to the proper representation of the physical phenomena.

Comparison of the Solid-Vortex Type of Swirl

The experimental data of McDonald et al.[6] are used for comparison. The configuration is a turbulent flow inside a conical diffuser of the total divergence angle of 8 deg and area ratio of 4.48. The measured circumferential velocity profile at the inlet is a linear function of radius over 80% of the radius and the swirl is the solid-vortex type except at the diffuser wall region. The measurements were made at a Reynolds number of approximately 1.5×10^5. Measured profiles of axial and tangential velocity components at the diffuser inlet are used for the calculation. Figures 7 and 8 show the predicted axial

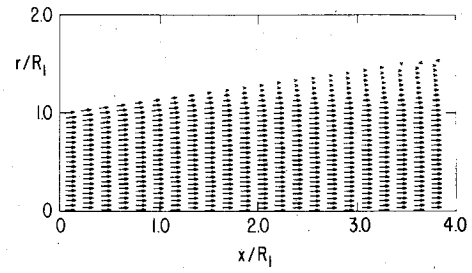

Fig 10a Development of axial velocity profile without a flow control ring.

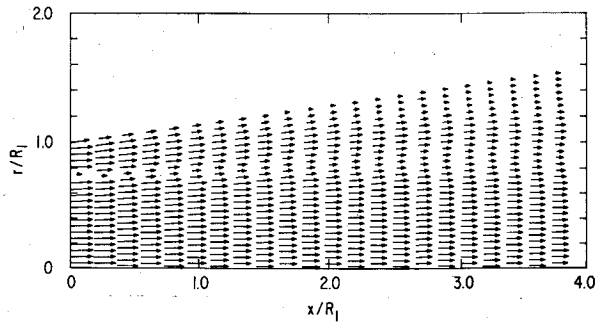

Fig. 10b Development of axial velocity profile with a flow control ring.

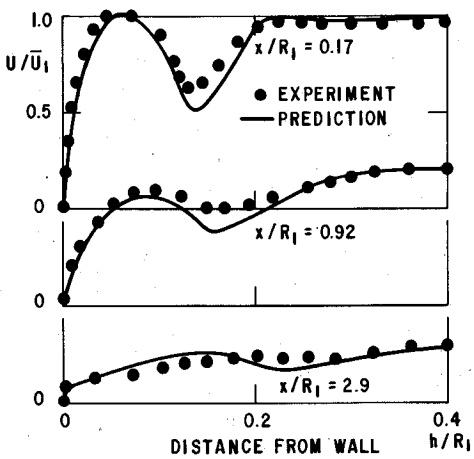

Fig. 11 Comparison for the velocity profile with a flow control ring.

and circumferential velocity profiles with 50×40 grid. With the swirl components, the maximum axial velocity occurs away from the diffuser centerline. The effects of the inlet swirl on the wall boundary-layer development are well shown and the experimental data are very well predicted. Figure 9 shows the comparison of the diffuser performance coefficient defined as

$$C_{prs}=\frac{1/A_2\int p_2 dA_2-1/A_1\int p_1 dA_1}{\tfrac{1}{2}\rho(1/A_1)\int U_1^2 dA_1} \tag{17}$$

Predictions with three different computational grids are compared with the experimental data in Fig. 9. The same stretching function is used for all of the grids. The flows with additional amounts of swirl (up to an inlet swirl angle of 45 deg) are also numerically simulated and the predicted results are compared. With the additional swirl, reversed flow region was observed near the centerline at the exit and lower pressure recovery is predicted. The predicted results indicate that the optimum amount of swirl for the diffuser configuration is about 20-25 deg, which the experimental study, unfortunately, did not pursue. When insufficient grid size is used, thicker boundary-layer development is predicted on the diffuser wall and lower pressure recovery is obtained. Also, the optimum amount of swirl is overpredicted with the smaller grid size.

Comparisons of the Inlet Distortion Effects

Various experimental studies have indicated that certain types of separation and transitory stall in "clean" diffusers can be avoided by changing the inlet flow conditions. The experimental data of Sajben et al.[9] were used to examine whether this kind of flow could be numerically calculated. The configuration is a conical diffuser with a total expansion angle of 16 deg and area ratio of 2.4. To alter the inlet flow conditions, a thin ring (thickness = $0.03\times$ inlet radius) was located outside of the wall boundary layer at the inlet. The developments of the velocity profiles with and without the flow control ring are compared in Fig. 10. The calculation uses 50×50 grids and three nodes are used to simulate the flow control ring. Figure 11 shows the comparison between the measured and the predicted velocity profiles. The separation near the wall is suppressed when the inlet flow is altered with the flow control ring. This is due to the more favorable pressure gradient along the wall and the higher diffuser performance thus obtained. The numerical calculation predicts all of these effects clearly and can be used to provide guiding information for the advanced design.

V. Conclusions

Turbulent flows inside various diffusers with the effects of inlet swirl and inlet distortion have beeen numerically predicted. Higher order discretization schemes have been applied to reduce the numerical diffusion and an algebraic Reynolds stress model modified for the streamline curvature was used. The important conclusions drawn from this study are:

1) The general features of the diffuser flows with inlet swirl and inlet distortion are properly predicted when a higher order discretization scheme is used for the convection term and the effect of the streamline curvature is properly included in the turbulence closure modeling.

2) The hybrid discretization scheme for the convection term introduces substantial numerical diffusion and underpredicts the separated zone and the recirculating zone near the diffuser centerline. The higher order discretization schemes provide a grid-independent solution with fewer grid nodes. Unless unrealistically fine grids are used, the hybrid discretization scheme cannot be used to obtain a reliable prediction even for engineering purposes.

3) The standard k-ϵ model does not represent the general flow development accurately and overestimates the diffuser performance when the inlet flow has a strong swirl component. With the stronger swirl, the overall curvature effect increases and the discrepancy between the predicted and measured velocity profiles are observed. With the curvature-modified algebraic Reynolds stress model, the correct trend is well predicted with the accuracy acceptable for engineering practice.

4) The complex turbulent flows inside various diffusers under the effects of the inlet swirl and the inlet distortion at high Reynolds number can be predicted numerically and the numerical calculation provides useful guidance for the design purpose.

References

[1] Kline, S. J., Abbott, D. E., and Fox, R. W., "Optimum Design of Straight Walled Diffusers," *Journal of Basic Engineering*, Vol. 81, Sept. 1959, p. 321.

[2] Sovran, G. and Klomp, E. D., "Experimentally Determined Optimum Geometries for Rectilinear Diffusers with Rectangular, Conical, or Annular Cross Section," *Fluid Mechanics of Internal Flow*, edited by G. Sovran, Elsevier Publishing Co., Amsterdam, the Netherlands, 1967, pp. 270-319.

[3] Bradley, C. I. and Cockrell, D. J., "The Response of Diffusers to Conditions at Their Inlet," Paper 5, Sec. A, presented at Symposium on Internal Flows, University of Salford, Salford, England, 1971.

[4] Ghose, S. and Kline, S. J., "Prediction of Transitory Stall in Two-Dimensional Diffusers," Thermosciences Division, Dept. of Mechanical Engineering, Stanford University, Stanford, Calif., Rept. MD-36, Dec. 1976.

[5] Bardina, J., Lyrio, A., Kline, S. J., Ferziger, J. H., and Johnston, J. P., "A Prediction Method for Planar Diffuser Flows," *Journal of Fluid Engineering,* Vol. 103, June 1981, pp. 315-321.

[6] McDonald, A. T., Fox, R. W., and Van Dewoestine, R. V., "Effects of Swirling Inlet Flow on Pressure Recovery in Conical Diffusers," *AIAA Journal,* Vol. 9, Oct. 1971, p. 2014.

[7] Senoo, Y., Kawaguchi, N., and Nagata, T., "Swirl Flow in Conical Diffusers," *Bulletin of Japan Society of Mechanical Engineers,* Vol. 21, No. 151, 1978, pp. 112-119.

[8] Moore, C. A. and Kline, S. J., "Some Effects of Vanes and of Turbulence in Two-Dimensional Wide-Angle Subsonic Diffusers," NACA TN 4080, 1958.

[9] Sajben, M., Chen, C. P., and Kroutel, J. C., "A New Passive Boundary Layer Control Device," *Journal of Aircraft,* Vol. 14, July 1977, pp. 654-660.

[10] Hoffmann, J. A., "Effects of Freestream Turbulence on Diffuser Performance," *Transactions of ASME, Journal of Fluids Engineering,* Vol. 103, Sept. 1981, pp. 388-390.

[11] de Vahl Davis, G. and Mallinson, G. D., "An Evaluation of Upwind and Central Difference Approximations by a Study of Recirculating Flow," *Computers and Fluids,* Vol. 4, 1976, pp. 29-43.

[12] Raithby, G. D., "A Critical Evaluation of Upstream Differencing Applied to Problems Involving Fluid Flow," *Computer Methods in Applied Mechanics and Engineering,* Vol. 9, 1976, pp. 75-103.

[13] Leschziner, M. A., "Practical Evaluation of Three Finite-Difference Schemes for the Computation of Steady State Recirculating Flows," *Computer Methods in Applied Mechanics and Engineering,* Vol. 23, 1980, pp. 293-312.

[14] Durst, F. and Rastogi, A. K., "Turbulent Flow Over 2D-Fences," *Turbulent Shear Flows,* Vol. 2, Springer Verlag, New York, 1980.

[15] Leschziner, M. A. and Rodi, W., "Calculation of Annular and Twin Parallel Jets Using Various Discretization Schemes and Turbulence Model Variations," *Transactions of ASME, Journal of Fluids Engineering,* Vol. 103, June 1981, pp. 352-360.

[16] Hah, C. and Lakshminarayana, B., "Prediction of Two- and Three-Dimensional Asymmetric Turbulent Wakes, Including Curvature and Rotation Effects," *AIAA Journal,* Vol. 18, Oct. 1980, pp. 1196-1204.

[17] Hah, C. and Lakshminarayana, B., "The Computation of a Highly Curved Mixing Layer with an Algebraic Reynolds Stress Closure Scheme," *Proceedings of the 1980-1981 AFOSR-HTTM-Stanford Conference on Complex Turbulent Flows.*

[18] Patankar, S. V., "Numerical Prediction of Three-Dimensional Flows," *Studies in Convection,* Vol. 1, edited by B. E. Launder, Academic Press, New York, 1975, p. 1.

[19] Gosman, A. D. and Pun, W. M., "Calculation of Recirculating Flows," Dept. of Mechanical Engineering, Imperial College, London, Rept. HTS/74/2, 1974.

[20] Leonard, B. P., "A Stable and Accurate Convective Modeling Procedure Based on Quadratic Upstream Interpolation," *Computer Methods in Applied Mechanics and Engineering,* Vol. 19, 1979, pp. 59-98.

[21] Raithby, G. D., "Skew-Upwind Differencing Schemes for Problems Involving Fluid Flow," *Computer Methods in Applied Mechanics and Engineering,* Vol. 9, 1976, pp. 153-164.

[22] Harvey, J. K., "Some Observations of the Vortex Breakdown Phenomenon," *Journal of Fluid Mechanics,* Vol. 14, Pt. 4, Dec. 1962, pp. 585-592.

[23] So, Kwan L., "Vortex Phenomena in a Conical Diffuser," *AIAA Journal,* Vol. 5, June 1967, pp. 1072-1078.